ELSEVIER

Journal of Nuclear Materials 245 (1997) 1–9

journal of nuclear materials

# Incorporation mechanisms of actinide elements into the structures of $U^{6+}$ phases formed during the oxidation of spent nuclear fuel

Peter C. Burns [1], Rodney C. Ewing *, Mark L. Miller

*Department of Earth and Planetary Sciences, University of New Mexico, Albuquerque, NM 87131-1116, USA*

Received 30 July 1996; accepted 6 January 1997

**Abstract**

Uranyl oxide hydrate and uranyl silicate phases will form due to the corrosion and alteration of spent nuclear fuel under oxidizing conditions in silica-bearing solution. The actinide elements in the spent fuel may be incorporated into the structures of these secondary $U^{6+}$ phases during the long-term corrosion of the $UO_2$ in spent fuel. The incorporation of actinide elements into the crystal structures of the alteration products may decrease actinide mobility. The crystal chemistry of the various oxidation states of the actinide elements of environmental concern is examined to identify possible incorporation mechanisms. The substitutions $Pu^{6+} \leftrightarrow U^{6+}$ and $(Pu^{5+}, Np^{5+}) \leftrightarrow U^{6+}$ should readily occur in many $U^{6+}$ structures, although structural modification may be required to satisfy local bond-valence requirements. Crystal-chemical characteristics of the $U^{6+}$ phases indicate that $An^{4+}$ (An: actinide) $\leftrightarrow U^{6+}$ substitution is likely to occur in the sheets of uranyl polyhedra that occur in the structures of the minerals schoepite, $[(UO_2)_8O_2(OH)_{12}](H_2O)_{12}$, ianthinite, $[U_2^{4+}(UO_2)_4O_6(OH)_4(H_2O)_4](H_2O)_5$, becquerelite, $Ca[(UO_2)_3O_2(OH)_3]_2(H_2O)_8$, compreignacite, $K_2[(UO_2)_3O_2(OH)_3]_2(H_2O)_8$, α-uranophane, $Ca[(UO_2)(SiO_3OH)]_2(H_2O)_5$, and boltwoodite, $K(H_3O)[(UO_2)(SiO_4)]$, all of which are likely to form due to the oxidation and alteration of the $UO_2$ in spent fuel. The incorporation of $An^{3+}$ into the sheets of the structures of α-uranophane and boltwoodite, as well as interlayer sites of various uranyl phases, may occur.

## 1. Introduction

The $UO_2$ in spent nuclear fuel typically contains 95 to 99% $UO_2$, up to 1% Pu, and up to 4% other actinides and fission products [1]. Under oxidizing conditions, such as those found in the proposed nuclear waste repository at Yucca Mountain, Nevada, $UO_2$ is unstable and the alteration rate is likely to be appreciable [2]. $U^{6+}$ minerals and other inorganic phases have received increased attention because they form as alteration products on uraninite ($UO_{2+x}$) under oxidizing conditions [3,4] and on $UO_2$ and spent fuel in experimental studies [5–10]. Recent results of experiments on the oxidative dissolution of spent fuel indicate fission products such as $^{137}Cs$ and $^{90}Sr$, and actinides such as Pu, are being incorporated into the alteration products [7]. Thus, the oxidized alteration products, mainly $U^{6+}$ phases, may play an important role in the release of radionuclides from the spent fuel.

The radioactivity and toxicity of long-lived actinide elements contained in spent fuel is a cause for concern if they are released into the environment [11]. Oversby [12] identifies Th, U, Np, Pu, Am and Cm as important elements for spent fuel disposal. Transport of these nuclides in solution will be the principal mechanism of release from the spent fuel [2]. The oxidation states of these 5f elements can be highly variable due to the screening of the 5f electrons from the nucleus. Under oxidizing conditions the elements can form complexes with a wide variety of inorganic and organic ligands, causing the mobilities to increase. Under oxidizing conditions the ions of environmental concern may include $Th^{4+}$, $U^{4+,6+}$, $Np^{4+,5+}$, $Pu^{3+,4+,5+,6+}$, $Am^{3+}$ and $Cm^{3+}$ [11].

As a result of the oxidation of spent fuel, $U^{6+}$ phases will form. Depending on the composition of the fluid

* Corresponding author.

[1] Present address: Department of Geology, University of Illinois, 1301 W. Green Street, Urbana, IL 61801, USA.

0022-3115/97/$17.00 Copyright © 1997 Elsevier Science B.V. All rights reserved.
*PII* S0022-3115(97)00006-8

phase, these will be uranyl oxide hydrates, uranyl carbonates, uranyl silicates or uranyl phosphates. Studies of $UO_2$ exposed to silica-rich ground water showed that the $UO_2$ altered progressively to uranyl oxide hydrates, then to uranyl silicates and alkali and alkaline-earth uranyl silicates [5]. These same phases are also found as alteration products of uraninite in uranium deposits [3,4]. The crystal structures of the $U^{6+}$ phases are complex, and it is only recently that a systematic hierarchy of the structures of these ~ 180 phases has been developed [13].

The actinides contained in the spent fuel (Th, U, Np, Pu, Am and Cm) will be released during the oxidation and dissolution of the $UO_2$ matrix, and their mobility will be strongly influenced by their abilities to be incorporated in the crystal structures of $U^{6+}$ phases, which form as alteration products of $UO_2$. The relatively low concentrations of the transuranium elements in spent fuel will preclude the formation of separate, pure phases [12]. The incorporation of relatively small quantities of the actinide elements into the uranyl phases may therefore impact upon their mobility. The purpose of this paper is to identify crystal-chemically feasible incorporation mechanisms of actinide elements into the structures of uranyl phases; this should be a useful aid in constraining future experimental investigations and identifying relevant crystal structures.

## 2. The crystal-chemistry of $U^{6+}$

A detailed understanding of the crystal chemistry of $U^{6+}$ is necessary to evaluate the likelihood of the incorporation of actinide elements in low concentrations into the structures of $U^{6+}$ phases. The $U^{6+}$ cation usually occurs in crystal structures as part of an approximately linear $(U^{6+}O_2)^{2+}$ uranyl ion (Fig. 1) [14]. The $U^{6+}$–O bond-lengths of the uranyl ion are ~ 0.18 nm, thus the bond-valence requirements of the uranyl-ion oxygen-atoms (hereafter referred to as $O_{Ur}$) are largely satisfied without further bonding. The uranyl ion occurs in crystal structures coordinated by four, five or six anions in an approximately planar arrangement perpendicular to the uranyl ion, giving Ur$\phi_4$ square, Ur$\phi_5$ pentagonal, and Ur$\phi_6$ hexagonal bipyramids (Ur: uranyl ion, $\phi$: $O^{2-}$, $OH^-$, $H_2O$), respectively (Fig. 1). The uranyl ion is not always present in polyhedra where the $U^{6+}$ is coordinated by six anions; both octahedral and distorted octahedral coordination geometries also occur [15]. Burns et al. [15] have examined the details of bond-length variations in $U^{6+}$ coordination polyhedra in well-refined structures. Where the uranyl ion is present, $\langle U^{6+}–O_{Ur}\rangle$ and $\langle U^{6+}–\phi_{eq}\rangle$ ($\phi_{eq}$: equatorial $\phi$) bond-lengths for Ur$\phi_4$ polyhedra are 0.179 ($\sigma = 0.003$) and 0.228 ($\sigma = 0.005$) nm, respectively. Uranyl ions are always present in $^{[7]}U^{6+}$ and $^{[8]}U^{6+}$ polyhedra [15]. For Ur$\phi_5$ polyhedra, $\langle U^{6+}–O_{Ur}\rangle$ is 0.179 ($\sigma = 0.004$) nm and $\langle U^{6+}–\phi_{eq}\rangle$ is 0.237 ($\sigma = 0.009$) nm. For Ur$\phi_6$ polyhedra, $\langle U^{6+}–O_{Ur}\rangle$ is 0.178 ($\sigma = 0.003$) nm and $\langle U^{6+}–\phi_{eq}\rangle$ is 0.247 ($\sigma = 0.012$) nm. The uranyl ion is often linear, and the O–U–O bond-angle of the uranyl ion seldom diverges more than 5° from linearity.

The uranyl ion has a formal valence of 2+, thus typical bond-valences associated with each $U^{6+}–\phi_{eq}$ bond are ~ 0.5, ~ 0.4 and ~ 0.33 vu for Ur$\phi_4$, Ur$\phi_5$ and Ur$\phi_6$ polyhedra, respectively. As the bond-valence requirements of the equatorial anions are only partially satisfied by the $U^{6+}–\phi_{eq}$ bond, Ur$\phi_n$ polyhedra may polymerize with other Ur$\phi_n$ polyhedra or with other cation polyhedra to form complex structures without violating the valence-sum rule [16]. Because the equatorial anions are close to co-planar, and the $O_{Ur}$ bond-valence requirements are satisfied without substantial further bonding, the sharing of Ur$\phi_n$ polyhedron equatorial-edges and corners commonly results in structures with infinite sheets. In such cases the uranyl ion is oriented approximately perpendicular to the sheet, and the sheets are most often connected through weaker bonds to interlayer cations and through hydrogen bonds to interlayer $H_2O$ groups.

A total of 106 $U^{6+}$ structures was classified as sheet structures by Burns et al. [13]. Sheets were compared and grouped on the basis of the topological arrangement of the anions that occur within the sheet [13,17]. The procedure for obtaining the anion topology of a sheet of polyhedra is given in Fig. 2. All anion topologies may be regarded as orderly arrays of edge-sharing, space-filling polygons with translational symmetry. Twenty-nine unique anion-topologies were identified by Burns et al. [13].

Each polygon in an anion topology corresponds to a potential cation site. For example, the center of a triangle

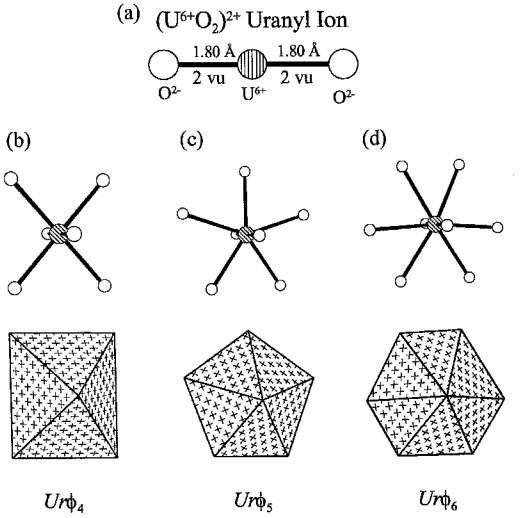


Fig. 1. The three types of Ur$\phi_n$ polyhedra (Ur: uranyl ion, $\phi$: unspecified anion). $U^{6+}$ cations are shown as circles shaded with parallel lines, and anions are shown as open circles. (a) Uranyl ion, (b) square bipyramid, (c) pentagonal bipyramid, (d) hexagonal bipyramid.

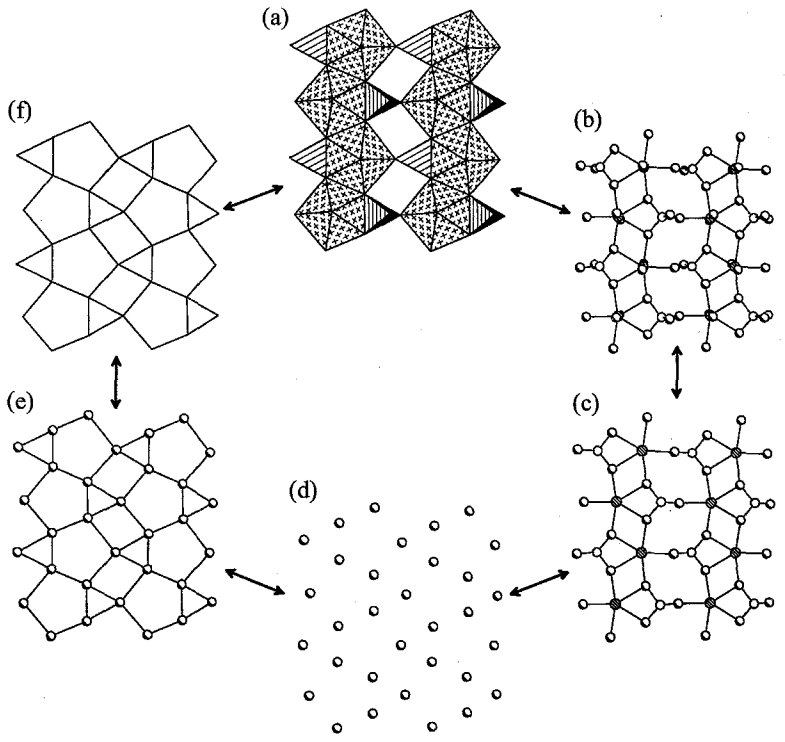


Fig. 2. The procedure for obtaining a sheet anion-topology that corresponds to a sheet of polyhedra [13]. (a) The sheet of polyhedra. (b) A ball-and-stick representation of the sheet. (c) The sheet with all anions that are not bonded to two or more cations within the sheet, and are not an equatorial anion of a pyramid or bipyramid, removed. (d) The sheet with all cations, and cation–anion bonds, removed. (e) The sheet with anions connected. (f) The anion topology of the sheet.

may be populated by a carbon, nitrogen or boron atom, all of which occur in triangular coordination, or by a cation in triangular-bipyramidal coordination, or the triangle may be the face of a tetrahedron, etc. A square may be populated by a cation in tetrahedral coordination, with all four anions bonded within the sheet, or by a cation in square-planar, square-pyramidal or octahedral coordination.

Consideration of the 180 structures containing $U^{6+}$ classified by Burns et al. [13] permits the formulation of a number of rules which govern the population of the 29 anion topologies that form sheets [15]. These rules will be useful for determining where fission products and actinide elements may be accommodated in the structures of $U^{6+}$ phases [15].

(1) Ur$\phi_4$ polyhedra often share only corners with other uranyl polyhedra, and where Ur$\phi_4$ polyhedra share edges with other uranyl polyhedra, they are almost invariably with other Ur$\phi_5$ polyhedra.

(2) No structure contains either Ur$\phi_5$ or Ur$\phi_6$ polyhedra that only share corners with other uranyl polyhedra; where polymerization occurs, it involves the sharing of edges between polyhedra.

(3) Ur$\phi_5$ polyhedra most often share edges with other Ur$\phi_5$ polyhedra, although sharing of edges with both Ur$\phi_4$ or Ur$\phi_6$ polyhedra is common.

(4) Ur$\phi_6$ polyhedra often share edges with either Ur$\phi_5$ or Ur$\phi_6$ polyhedra, but never with Ur$\phi_4$ polyhedra.

(5) The most important factor in determining the mode of polymerization between Ur$\phi_n$ polyhedra and other cation polyhedra is cation charge.

(6) Cation polyhedra (excluding $U^{6+}$ polyhedra) with high cation charge $(6+)$ and low coordination number $(<6)$ usually do not share edges with Ur$\phi_n$ polyhedra.

(7) Polyhedra containing pentavalent cations commonly share edges with Ur$\phi_5$ and Ur$\phi_6$ polyhedra, but they also often share only corners with Ur$\phi_n$ polyhedra.

(8) Cation polyhedra with lower cation-charges $(\leq 4)$ almost always share edges with Ur$\phi_5$ or Ur$\phi_6$ polyhedra, but never with Ur$\phi_4$ polyhedra.

(9) An important geometric factor for determining structural connectivity is the edge-length mismatch of the ideal polyhedra, which is mainly due to cation size; small degrees of mismatch of the ideal polyhedral edge-lengths favors the sharing of edges; whereas, larger mismatch favors the sharing of corners only.

## 3. Incorporation mechanisms

The actinide elements (in addition to U) in spent nuclear fuel which are of the most environmental concern are

$Th^{4+}$, $Np^{4+,5+}$, $Pu^{3+,4+,5+,6+}$, $Am^{3+}$ and $Cm^{3+}$ [11]. The extent to which these elements can be incorporated into $U^{6+}$ phases effects their mobility. The electronic structure of these cations (excluding $Th^{4+}$) involves the filling of 5f orbitals, and as such, the coordination polyhedra typical of each cation are strongly influenced by cation charge. For cation charges 5 + (Np, Pu, Am) and 6 + (U, Np, Pu, Am), a linear $(An^{5+,6+}O_2)^{1+,2+}$ (An: actinide) actinyl ion dominates the coordination chemistry [18], and the coordination polyhedra are similar to those found for the $U^{6+}$ cation. When the cation charge is less than 5 +, a more regular polyhedron is typical. Thus, the oxidation state of the actinide element is of critical importance in identifying possible incorporation mechanisms into the structures of $U^{6+}$ phases.

Almost all of the $U^{6+}$ phases that will form due to the oxidative dissolution of $UO_2$ have structures that contain infinite sheets of polyhedra, although the presence of significant $CO_2$ can stabilize structures that contain finite clusters of $Ur\phi_6$ and $CO_3$ polyhedra. In most $U^{6+}$ phases that have sheet structures, all cations of higher bond-valence occur within the sheet; whereas, interlayer species are typically mono- or divalent cations and/or $H_2O$ groups. The substitution of actinide elements into $U^{6+}$ sheet structures may occur in any of three ways:

(1) Substitution for $U^{6+}$ by actinides within the sheet, together with appropriate charge-balancing mechanisms where required;

(2) Substitution for cations other than $U^{6+}$ either within the sheet or the interlayer, together with appropriate charge-balancing substitutions where necessary;

(3) Occupation of vacant sites by actinides either within the sheet or interlayer, together with appropriate charge-balancing substitutions.

### 3.1. Incorporation of $Np^{5+}$, $Pu^{5+}$, $Pu^{6+}$

Only a small number of crystal structures is known that contain $Np^{5+}$, $Pu^{5+}$ or $Pu^{6+}$; these are listed in Table 1. In all cases, the $Np^{5+}$ cation is part of a near-linear $(Np^{5+}O_2)^{1+}$ ion. Reported $Np^{5+}$–O bond-lengths in the $(Np^{5+}O_2)^{1+}$ ion range from 0.165 to 0.190 nm, with an average $\langle Np^{5+}–O\rangle$ of 0.181 nm and a standard deviation of 0.006 nm. Like the uranyl ion, the $(Np^{5+}O_2)^{1+}$ ion is coordinated by four, five and six anions, forming square, pentagonal and hexagonal bipyramids, respectively. When coordinated by $\phi$ ($O^{2-}$, $OH^-$, $H_2O$), the $\langle Np^{5+}–\phi_{eq}\rangle$ bond-length is ~ 0.010 nm longer than $\langle U^{6+}–\phi_{eq}\rangle$ bond-lengths in $Ur\phi_n$ polyhedra.

Only a small number of structures that contain $Pu^{5+}$ or $Pu^{6+}$ are known (Table 1). Only two known structures contain $Pu^{5+}$ and in both cases the $Pu^{5+}$ cation is part of a linear $(Pu^{5+}O_2)^{1+}$ ion. The $\langle Pu^{5+}–O\rangle$ bond-length in the $(Pu^{5+}O_2)^{1+}$ ion is 0.194 nm, and each $(Pu^{5+}O_2)^{1+}$ ion is coordinated by six oxygen atoms, forming hexagonal bipyramids. Only one refined structure contains $Pu^{6+}$ (Table 1). The $Pu^{6+}$ cation is part of a linear $(Pu^{6+}O_2)^{2+}$ ion, and the $Pu^{6+}$–O bond-length in the $(Pu^{6+}O_2)^{2+}$ ion is 0.190 nm. The $(Pu^{6+}O_2)^{2+}$ ion is coordinated by six oxygen atoms, giving a hexagonal bipyramidal polyhedron.

The close geometrical similarities of $Np^{5+}\phi_n$, $Pu^{5+}\phi_n$ and $Pu^{6+}\phi_n$ polyhedra with $Ur\phi_n$ polyhedra suggest that $Np^{5+}$, $Pu^{5+}$ and $Pu^{6+}$ should readily substitute for $U^{6+}$ in

Table 1
$Np^{5+}\phi_n$, $Pu^{5+}\phi_n$ and $Pu^{6+}\phi_n$ polyhedral bond-lengths in inorganic structures

| | Site | $Np^{5+}$ [a]–O (nm) | | Equatorial $Np^{5+}$–O (nm) | | | | | | Ref. |
|---|---|---|---|---|---|---|---|---|---|---|
| $Cs_3Np^{5+}O_2(SO_4)_2(H_2O)_2$ | Np(1) | 0.182 | 0.182 | 0.239 | 0.239 | 0.252 | 0.246 | 0.245 | | [37] |
| $K_4(H_5O_2)(Np^{5+}O_2)_3(Mo^{6+}O_4)_4(H_2O)_4$ | Np(1) | 0.184 | 0.184 | 0.239 | 0.239 | 0.239 | 0.239 | | | [19] |
| | Np(2) | 0.190 | 0.185 | 0.241 | 0.241 | 0.244 | 0.243 | 0.245 | | |
| $(Np^{5+}O_2)_2(NO_3)_2(H_2O)_5$ | Np(1) | 0.184 | 0.184 | 0.242 | 0.250 | 0.250 | 0.246 | 0.245 | | [38] |
| | Np(2) | 0.185 | 0.183 | 0.248 | 0.242 | 0.259 | 0.260 | 0.260 | 0.264 | |
| | | | | Equatorial $Np^{5+}$–Cl (nm) | | | | | | |
| $Cs(Np^{5+}O_2Cl_2(H_2O))$ | Np(1) | 0.180 | 0.181 | 0.249 | 0.284 | 0.287 | 0.287 | 0.287 | | [39] |
| $Cs_3(Np^{5+}Cl_4O_2)$ | Np(1) | 0.181 | 0.181 | | 0.275 | 0.275 | 0.276 | 0.276 | | [40] |
| $Cs_7(Np^{5+}O_2)(Np^{5+}O_2)_2Cl_{12}$ | Np(1) | 0.165 | 0.165 | | 0.268 | 0.268 | 0.268 | 0.268 | | [41] |
| $Cs_3(Np^{5+}O_2Cl_4)$ | Np(1) | 0.183 | 0.183 | | 0.276 | 0.276 | 0.276 | 0.276 | | [42] |
| | | $Pu^{5+}$ [a]–O (nm) | | Equatorial $Pu^{5+}$–O (nm) | | | | | | |
| $KPu^{5+}O_2CO_3$ | Pu(1) | 0.194 | 0.194 | 0.255 | 0.255 | 0.255 | 0.255 | 0.255 | 0.255 | [43] |
| $NH_4Pu^{5+}O_2CO_3$ | Pu(1) | 0.194 | 0.194 | 0.255 | 0.255 | 0.255 | 0.255 | 0.255 | 0.255 | [43] |
| | | $Pu^{6+}$ [a]–O (nm) | | Equatorial $Pu^{6+}$–O (nm) | | | | | | |
| $SrPu^{6+}O_4$ | Pu(1) | 0.190 | 0.190 | 0.235 | 0.235 | 0.235 | 0.235 | 0.235 | 0.235 | [44] |

[a] Actinyl ion.

Table 2
Selected $Th^{4+}$ $\phi_n$, $Np^{4+}$ $\phi_n$ and $Pu^{4+}$ $\phi_n$ polyhedral bond-lengths in inorganic structures

| | $Th^{4+}$–O (nm) | | | | | | | | | Ref. |
|---|---|---|---|---|---|---|---|---|---|---|
| $ThSiO_4$ | 0.281 | 0.250 | 0.257 | 0.252 | 0.239 | 0.243 | 0.242 | 0.241 | 0.251 | [45] |
| $KTh_2(VO_3)_3$ | 0.229 | 0.248 | 0.242 | 0.263 | 0.247 | 0.235 | 0.251 | 0.260 | 0.253 | [46] |
| $Th(MoO_4)_2$ | 0.239 | 0.238 | 0.243 | 0.241 | 0.242 | 0.238 | 0.246 | 0.236 | | [47] |
| $K_2Th(MoO_4)_3$ | 0.244 | 0.244 | 0.252 | 0.252 | 0.233 | 0.233 | 0.240 | 0.240 | | [48] |
| $NaK_3Th_2O_6$ | 0.232 | 0.232 | 0.233 | 0.233 | 0.235 | 0.235 | | | | [49] |
| | 0.237 | 0.237 | 0.235 | 0.235 | 0.233 | 0.233 | | | | |
| $ThO_2$ | 0.242 | 0.242 | 0.242 | 0.242 | 0.242 | 0.242 | | | | [50] |
| | $Np^{4+}$–O (nm) | | | | | | | | | |
| $Np^{4+}(VO_3)_4$ | 0.231 | 0.231 | 0.235 | 0.235 | 0.234 | 0.234 | 0.229 | 0.229 | | [51] |
| $Np^{4+}O_2$ | 0.235 | 0.235 | 0.235 | 0.235 | 0.235 | 0.235 | | | | [52] |
| $BaNp^{4+}O_3$ | 0.218 | 0.218 | 0.218 | 0.218 | 0.218 | 0.218 | | | | [36] |
| | $Pu^{4+}$–O (nm) | | | | | | | | | |
| $Pu^{4+}(SO_4)_2(H_2O)_4$ | 0.234 | 0.234 | 0.231 | 0.231 | 0.232 | 0.232 | 0.231 | 0.231 | | [53] |
| $BaPu^{4+}O_3$ | 0.222 | 0.222 | 0.223 | 0.223 | 0.223 | 0.223 | | | | [35] |
| $Pu^{4+}O_2$ | 0.234 | 0.234 | 0.234 | 0.234 | 0.234 | 0.234 | 0.234 | 0.234 | | [52] |

crystal structures, assuming local charge-balancing substitutions are possible (e.g., $O^{2-} \leftrightarrow OH^-$). However, the lower cation charge of $Np^{5+}$ and $Pu^{5+}$ may have important ramifications on the crystal structure as it results in lower bond-valence contributions to the oxygen atoms of the $(Np^{5+}O_2)^{1+}$ and $(Pu^{5+}O_2)^{1+}$ ions than required by the uranyl ion. The equatorial anions of the $Np^{5+}$ $\phi_n$ and $Pu^{5+}$ $\phi_n$ polyhedra require ~ 2 vu (as in Ur$\phi_n$ polyhedra), leaving only ~ 1.5 vu for each $Np^{5+}$–O or $Pu^{5+}$–O bond in the actinyl ion. For example, consider the structure of $K_4(H_5O_2)(NpO_2)_3(MoO_4)_4(H_2O)_4$ [19] which contains two symmetrically distinct Np sites. The Np(1) site is coordinated by six atoms of oxygen, and the $(Np^{5+}O_2)^{1+}$ ion contains two symmetrically equivalent O(1) atoms. Each O(1) atom is bonded to Np(1) as well as three K atoms. There are no bond-valence parameters available for $Np^{5+}$, but the sum of bond-valences to the three K atoms (calculated using the parameters of Brese and O'Keeffe [20]) is 0.46 vu, thus the $Np^{5+}$–O(1) bond is ~ 1.54 vu. The Np(2) site is coordinated by seven atoms of oxygen, and the O(2) atom of the $(Np^{5+}O_2)^{1+}$ ion also bonds to one K atom (0.10 vu) and one Np(1) atom (~ 0.4 vu), thus the Np(2)–O(2) bond is ~ 1.5 vu. Unlike uranyl polyhedra, where the $O_{Ur}$ bond-valence requirements are nearly satisfied by the $U^{6+}$–O bond, the $(Np^{5+}O_2)^{1+}$ and $(Pu^{5+}O_2)^{1+}$ ion oxygen-atoms require additional bonding. The coupled substitution $(U^{6+}, O^{2-}) \leftrightarrow (Np^{5+}, OH^-)$, $(Pu^{5+}, OH^-)$ provides both a charge-balancing mechanism and the possibility of satisfying local bond-valence requirements with hydrogen bonds.

### 3.2. Incorporation of $An^{4+}$ and $An^{3+}$

The $An^{4+}$ cations of interest here are $Th^{4+}$, $Np^{4+}$ and $Pu^{4+}$. Only a small number of structures are known that contain $Np^{4+}$ or $Pu^{4+}$, but numerous structures that contain $Th^{4+}$ have been determined. A selection of $An^{4+}$ polyhedral bond-lengths are listed in Table 2. The $An^{4+}$ cations show a strong tendency to be eight-coordinated, although coordination polyhedra containing from six to nine anions are known to occur. The bonding to the $An^{4+}$ cations does not tend to be polarized, and the coordination polyhedra are usually quite regular. Estimates of bond lengths from sums of effective ionic-radii [21] are: $^{[6]}Th^{4+}$–O = 0.230, $^{[8]}Th^{4+}$–O = 0.241, $^{[6]}Np^{4+}$–O = 0.223, $^{[8]}Np^{4+}$–O = 0.234, $^{[6]}Pu^{4+}$–O = 0.222, and $^{[8]}Pu^{4+}$–O = 0.232 nm; note that actinide contraction is evident.

Table 3
Selected $Pu^{3+}$ $\phi_n$ and $Am^{3+}$ $\phi_n$ polyhedral bond-lengths in inorganic structures

| | $Pu^{3+}$–O (nm) | | | | | | | | Ref. |
|---|---|---|---|---|---|---|---|---|---|
| $\beta$-$Pu_2^{3+}O_3$ | 0.264 | 0.264 | 0.264 | 0.231 | 0.231 | 0.231 | 0.241 | | [54] |
| | $Am^{3+}$–O (nm) | | | | | | | | |
| $(Am_2^{3+}(MoO_4)_3)_{1.333}$ | 0.248 | 0.248 | 0.248 | 0.248 | 0.246 | 0.246 | 0.246 | 0.246 | [55] |
| $Am_2^{3+}(SO_4)_3(H_2O)_8$ | 0.238 | 0.251 | 0.238 | 0.244 | 0.255 | 0.241 | 0.249 | 0.243 | [56] |
| $Am_2^{3+}O_3$ | 0.234 | 0.234 | 0.238 | 0.238 | 0.236 | 0.236 | | | [57] |

The $An^{3+}$ cations of interest here are $Pu^{3+}$, $Am^{3+}$ and $Cm^{3+}$. These cations tend to occur in regular polyhedra, usually coordinated by six or eight anions. Examples of polyhedral bond-lengths are given in Table 3. Typical bond-lengths for $An^{3+}$–O obtained from sums of effective ionic-radii [21] are: $^{[6]}Pu^{3+}$–O = 0.236, $^{[6]}Am^{3+}$–O = 0.233 and $^{[6]}Cm^{3+}$–O = 0.233 nm. It is important to note that the crystal chemistry of the $An^{3+}$ cations is quite similar to REE cations, although the REE cations are slightly larger than $An^{3+}$ cations.

### 3.2.1. Uranyl oxide hydrates

The earliest alteration products to form when $UO_2$ corrodes in contact with oxygen-rich ground water are uranyl oxide hydrates [5], and the structures of each of these phases are based upon sheets of uranyl polyhedra. In these structures, the high-valence cations are restricted to the sheets of polyhedra. The sheets are connected through low-valence interlayer cations, $H_2O$ groups, and through hydrogen bonds. The incorporation of $An^{4+}$ cations into these structures is therefore most likely to occur within the sheet of high bond-valence polyhedra, rather than in the interlayer.

The crystal-chemical behaviors of the $An^{4+}$ cations of interest here are similar to $U^{4+}$, which has an expected $^{[6]}U^{4+}$–O bond-length of 0.225 nm (from sums of effective ionic-radii [21]), a value similar to other $An^{4+}$–O bond-lengths. Consider the sheet that occurs in the structure of ianthinite, $[U_2^{4+}(UO_2)_4O_6(OH)_4(H_2O)_4](H_2O)_5$ [22] (Fig. 3a). This sheet, referred to as the $\beta$-$U_3O_8$ sheet [13], contains $Ur\phi_5$ and $U^{4+}\phi_6$ polyhedra, arranged such that the $Ur\phi_5$ polyhedra share edges to form parallel chains that are separated by the $U^{4+}\phi_6$ polyhedra. In the structure of ianthinite, the sheets of $Ur\phi_5$ and $U^{4+}\phi_6$ polyhedra are connected through hydrogen bonding to interlayer $H_2O$ groups. This sheet also occurs in the structures of $\beta$-$U_3O_8$ [23], where adjacent sheets are linked by shared anions, and billietite, $Ba[(UO_2)_3O_2(OH)_3]_2(H_2O)_4$ [24], where adjacent sheets are linked through Ba cations and $H_2O$ groups located in interlayer positions.

As the $\beta$-$U_3O_8$ sheet can accommodate large amounts of $U^{4+}$ as shown by the structure of ianthinite, and because the crystal chemistry of $Th^{4+}$, $Np^{4+}$ and $Pu^{4+}$ are similar to $U^{4+}$, we predict that the structures of ianthinite and billietite will accommodate considerable amounts of $Th^{4+}$, $Np^{4+}$ and $Pu^{4+}$. In the structure of ianthinite, $An^{4+} \leftrightarrow U^{4+}$ substitution can occur directly, but in the structure of billietite an additional charge-balancing substitution must also occur. One possible substitution is $OH^- \leftrightarrow O^{2-}$, and another possibility is the incorporation of additional low-valence cations (other than $H^+$). For example, the synthetic compound $Li_{0.88}U_3O_8$ [25] is also based upon the $\beta$-$U_3O_8$-type sheet (Fig. 3a), but $Li^+$ occurs between the sheets, maintaining charge balance as the oxidation state of the uranium varies relative to $U_3O_8$.

The sheet that occurs in the structure of $\alpha$-$U_3O_8$ [26] (Fig. 3b) is thought to contain both $U^{5+}$ and $U^{6+}$. As in the $\beta$-$U_3O_8$ sheet (Fig. 3a), this sheet contains parallel chains of edge-sharing $U\phi_7$ polyhedra, but in the $\alpha$-$U_3O_8$ sheet, the chains are separated by $U\phi_7$ polyhedra, rather than $U\phi_6$ polyhedra. Sheets with the same connectivity are the basis of the structures of protasite, $Ba[(UO_2)_3O_3(OH)_2](H_2O)_3$ [24], billietite [24] (which also contains the sheet shown in Fig. 3a) and becquerelite, $Ca[(UO_2)_3O_2(OH)_3]_2(H_2O)_8$ [24]. The sheet almost certainly occurs in the structure of compreignacite, $K_2[(UO_2)_3O_2(OH)_3]_2(H_2O)_8$ [27], but the structure has not yet been fully resolved. As the $\alpha$-$U_3O_8$ sheet is sufficiently flexible to accommodate both $U^{5+}$ and $U^{6+}$ (and possibly $U^{4+}$, which cannot be excluded from $\alpha$-$U_3O_8$), we predict that the similar sheet in the structures of protasite, billietite, becquerelite and compreignacite are

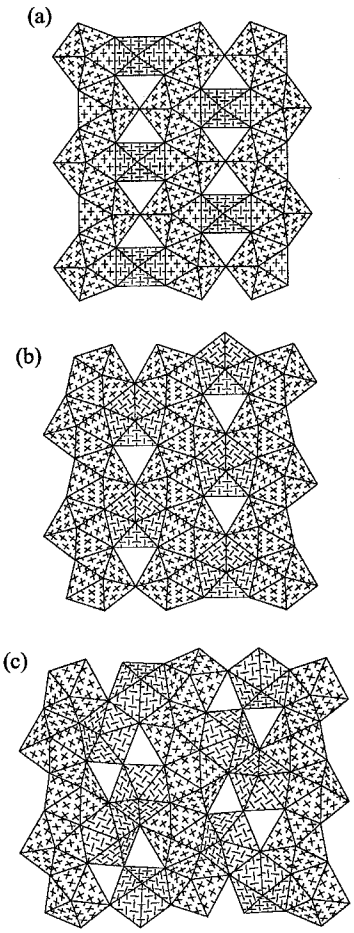


Fig. 3. Sheets of uranyl polyhedra that occur in the structures of: (a) ianthinite, $\beta$-$U_3O_8$ and billietite, (b) $\alpha$-$U_3O_8$, protasite, billietite and becquerelite, (c) schoepite and fourmarierite. Polyhedra belonging to the chain of edge-sharing pentagonal bipyramids are shaded with crosses, other polyhedra are shaded with a herringbone pattern.

likely to incorporate $Th^{4+}$, $Np^{4+}$ and $Pu^{4+}$, assuming that local charge-balancing substitutions occur. Experiments on the corrosion of $UO_2$ under oxidizing conditions using ground water have confirmed the formation of becquerelite and possibly compreignacite [5].

The structures of schoepite, $[(UO_2)_8O_2(OH)_{12}](H_2O)_{12}$ [28], and fourmarierite, $Pb[(UO_2)_4O_3(OH)_4](H_2O)_4$ [29], are both based upon the sheet shown in Fig. 3c. This sheet contains only $Ur\phi_5$ polyhedra and resembles the $\alpha$-$U_3O_8$ sheet shown in Fig. 3b. The sheet contains parallel chains of edge-sharing $Ur\phi_5$ polyhedra, separated by edge-sharing dimers of $Ur\phi_5$ polyhedra rather than the single $U\phi_7$ polyhedron that separates the chains in the $\alpha$-$U_3O_8$ sheet. Due to the similarity of these two sheets, we predict that it is likely that $Th^{4+}$, $Np^{4+}$ and $Pu^{4+}$ can be accommodated in the structures of schoepite and fourmarierite. In corrosion experiments of $UO_2$ with ground water, schoepite was probably one of the first phases to form [5]. Fourmarierite is unlikely to form as a corrosion product of young spent fuel due to the absence of radiogenic Pb.

$An^{3+}$ cations will probably not substitute for $U^{6+}$ in the crystal structures of uranyl oxide hydrates to any significant extent due to the disparity of charge. It is more plausible that $An^{3+}$ cations will substitute in the interlayer, either in place of other cations, or possibly in a vacant site. These cations will behave much like REEs and will generally be compatible with divalent cation polyhedra in the interlayer. For example, the $Ca^{2+}$ site in the structure of becquerelite ($Ca^{2+}$–O ~ 0.236 nm from sums of effective ionic-radii [21]) might accommodate $An^{3+}$ cations, assuming local charge-balancing substitutions occur.

### 3.2.2. *Uranyl silicates*

There are about fifteen uranyl silicate minerals, but the crystal structures have only been determined for eight of these. When $UO_2$ was experimentally corroded with silica-rich ground water, four uranyl silicate minerals formed [5]: $\alpha$-uranophane, $Ca[(UO_2)(SiO_3OH)]_2(H_2O)_5$, boltwoodite, $K(H_3O)[(UO_2)(SiO_4)]$, sklodowskite, $Mg[(UO_2)(SiO_3OH)]_2$, and soddyite, $(UO_2)_2(SiO_4)(H_2O)_2$. The structure of soddyite is a framework of edge-sharing $Ur\phi_5$ polyhedra and $Si\phi_4$ tetrahedra [30]. The structures of $\alpha$-uranophane [31], boltwoodite [32] and sklodowskite [33] all contain the uranyl silicate sheet shown in Fig. 4a. The sheet contains chains of edge-sharing $Ur\phi_5$ polyhedra that are cross-linked via $Si\phi_4$ tetrahedra, and the sheet anion-topology is shown in Fig. 4b.

In the uranophane anion-topology (Fig. 4b), pentagons share edges to form chains that are parallel, and adjacent chains of pentagons are separated by chains of alternating, edge-sharing triangles and squares. Sixteen structures contain sheets that are based upon this anion topology (not all are uranyl silicates), and there are ten distinct ways in which this anion topology is populated [13]. In all cases each of the pentagons in the anion topologies are populated; in fourteen structures all pentagons contain only $Ur\phi_5$ polyhedra, in the remaining two structures half of the pentagons are populated with $Ur\phi_5$ polyhedra and half are populated with $Ca\phi_8$ or $Na\phi_7$ polyhedra. This observation is important as it demonstrates that low-valence cations occur in the pentagons of this anion topology.

No sheet based upon the uranophane anion-topology has both the triangles and the squares populated. In one sheet the triangles are populated with $B\phi_3$ triangles, in four sheets the triangles are the faces of $Si\phi_4$, $As\phi_4$ or $P\phi_4$ tetrahedra, in one sheet all squares contain $Ur\phi_4$ polyhedra, in one sheet one half of the squares contain $Ur\phi_4$ polyhedra and the other half are vacant, in one sheet one half of the squares contain $Ur\phi_4$ polyhedra and one half contain $Cu\phi_6$ octahedra, in one sheet the squares are populated by distorted $Te\phi_4$ polyhedra, and in one sheet the squares are populated with $Nb\phi_5$ square-pyramids. Thus, it is apparent that the uranophane anion-topology is compatible with numerous compositions.

One possible location for the substitution of $An^{4+}$ or $An^{3+}$ cations in the uranophane sheet is the $Ur\phi_5$ polyhedron. Consider the sheet that occurs in the structure of ulrichite (Fig. 4c), $Cu[Ca(UO_2)(PO_4)_2](H_2O)_4$ [34], which

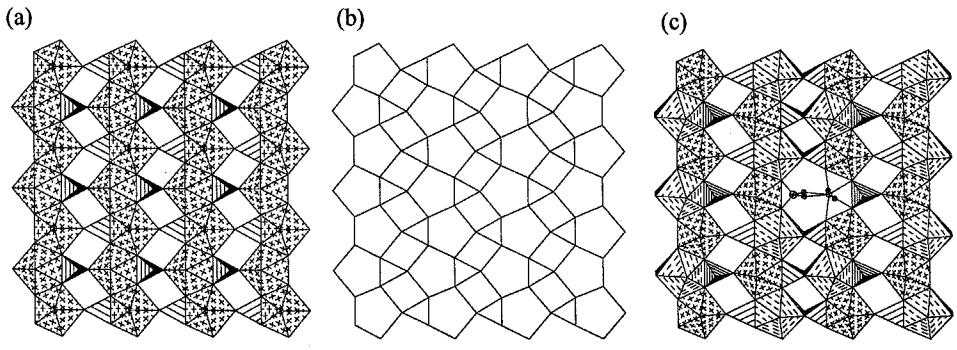


Fig. 4. Sheets of uranyl polyhedra and tetrahedral polyhedra that occur in the structures of: (a) $\alpha$-uranophane, boltwoodite and sklodowskite (and other uranyl silicate minerals), (c) ulrichite. Uranyl polyhedra are shaded with crosses, $Ca\phi_8$ polyhedra with broken lines and tetrahedra are shaded with parallel lines.

is based upon the uranophane anion-topology (Fig. 4b). The sheet contains $Ur\phi_5$ polyhedra, $Ca\phi_8$ polyhedra and $P\phi_4$ tetrahedra. In the α-uranophane sheet (Fig. 4a) only three of the anions of each tetrahedron are shared with $Ur\phi_5$ polyhedra. In contrast, the ulrichite sheet contains two types of $P\phi_4$ tetrahedra; in one type all anions are shared within the sheet, while the other tetrahedron only shares three anions within the sheet. Each $Ca\phi_8$ polyhedron shares two of its edges with $P\phi_4$ tetrahedra; one of these $P\phi_4$ tetrahedra also shares an edge with a $Ur\phi_5$ polyhedron; whereas, the other tetrahedron shares only a corner with a $Ur\phi_5$ polyhedron in an adjacent chain. The striking similarity of the α-uranophane and ulrichite sheets clearly demonstrates that it is possible to place low-valence cations in the $U^{6+}$ sites of the α-uranophane-type sheet, so long as the tetrahedron rotates so that the site becomes eight-coordinated (to satisfy local bond-valence requirements) and charge-balancing substitutions also occur.

The details of the $Si\phi_4$ tetrahedra in the structures of α-uranophane, boltwoodite and sklodowskite may be examined to determine if the tetrahedra can rotate sufficiently to create an eight-coordinated polyhedral geometry. The structure of α-uranophane contains two symmetrically distinct $Si\phi_4$ tetrahedra; $Si(1)\phi_4$ shares its non-sheet anion with an interlayer Ca cation, and in the case of $Si(2)\phi_4$, the non-sheet anion is a hydroxyl group that is hydrogen bonded to interlayer $H_2O$. Thus, the $Si(2)\phi_4$ tetrahedron may rotate. The structure of boltwoodite contains only one symmetrically distinct $Si\phi_4$ tetrahedron. The apical ligand of the tetrahedron is a hydroxyl group which is also weakly bonded to a K cation in the interlayer at a distance of 0.315 nm. The $Si\phi_4$ tetrahedron may therefore rotate. Finally, the structure of sklodowskite contains one symmetrically distinct $Si\phi_4$, but the apical anion bonds to $Mg^{2+}$ in the interlayer, thus the tetrahedron is not as likely to rotate. $An^{4+}$ and $An^{3+}$ cations can reasonably be expected to substitute for $U^{6+}$ in the α-uranophane sheet, as their coordination polyhedra are geometrically similar to $Ca\phi_8$ polyhedra. However, due to local bonding constraints, significant substitution in these three uranyl silicates will probably be limited to α-uranophane and boltwoodite.

Consideration of the geometry of the uranophane anion-topology (Fig. 4b) suggests that the square sites may be populated by $An^{4+}\phi_6$ octahedra. $An^{4+}\phi_6$ octahedra occur in the structures of $BaPu^{4+}O_3$ [35] and $BaNp^{4+}O_3$ [36], and the polyhedral size is approximately compatible with the squares in the anion topology. Also, several structures are known that contain sheets that are based upon the uranophane anion-topology that have the square sites populated with $Ur\phi_4$, $Cu^{2+}\phi_6$, $Te^{4+}\phi_4$ and $Nb^{5+}\phi_5$ polyhedra. However, no sheet based upon this anion topology has both the squares and the triangles populated, presumably because this would violate the valence-sum rule [16] at the anion positions. Therefore, the incorporation of $An^{4+}$ at the square sites in the anion topology requires that adjacent $Si\phi_4$ tetrahedra are vacant. This could be achieved by the substitution $(Si^{4+}O^{2-}) \leftrightarrow (An^{4+}(OH^-)_2)$, where the $Si^{4+}$ cation and non-sheet anion are replaced by an $An^{4+}$ cation and two hydroxyl groups in the adjacent square of the anion topology. This substitution seems less plausible than substitution of the $An^{4+}$ cation for $U^{6+}$ (discussed above).

As argued above for the uranyl oxide hydrate phases, it is also likely that substitution of $An^{3+}$ cations may occur for cations in the interlayer sites in the structures of uranyl silicates. The $An^{3+}$ polyhedra are generally compatible with large divalent cation polyhedra, such as the $Ca^{2+}$ site in α-uranophane.

## 4. Summary

The corrosion of the $UO_2$ in spent nuclear fuel under oxidizing conditions will result in the formation of uranyl oxide hydrates and uranyl silicates [3–10]. During the dissolution of the $UO_2$ matrix the actinide elements, Th, Np, Pu, Am and Cm, will potentially be released into solution. The crystal chemistry of the actinides has been used to examine whether it is reasonable to expect these nuclides to be incorporated into the structures of uranyl oxide hydrates and uranyl silicates. Based on an analyses of the known structures, the substitutions $Pu^{6+} \leftrightarrow U^{6+}$ and $(Np^{5+}, Pu^{5+}) \leftrightarrow U^{6+}$ are likely to occur in most $U^{6+}$ structures. Also, based on consideration of the crystal structures, we predict that $An^{4+}$ cations will readily substitute for $U^{6+}$ in the sheets that occur in the structures of schoepite, ianthinite, becquerelite, compreignacite, α-uranophane and boltwoodite, all of which are known to occur as the corrosion products of $UO_2$ treated with Si-rich ground water [5]. The substitution of $An^{3+}$ may occur at the interlayer sites, although $An^{3+}$ may also be accommodated in the sheets in the structures of α-uranophane and boltwoodite.

We emphasize that these conclusions are preliminary and confirmation will require experimental work, including structure determinations of An-substituted $U^{6+}$ phases and chemical analyses of the alteration products formed in experiments and nature.

## Acknowledgements

This work was supported by the Natural Sciences and Engineering Research Council of Canada with a Post-Doctoral Fellowship to PCB and the Office of Basic Energy Sciences of the US Department of Energy (Grant No. DE-FG03-95ER14540). R.C.E. acknowledges early support from the Swedish Nuclear Fuel and Waste Management Co. (SKB) that led the authors to this subject.

## References


[1] J.O. Barner, Pacific Northwest Laboratory Report PNL-5109 (1985).
[2] W.M. Murphy and R.T. Pabalan, Center for Nuclear Waste Regulatory Analyses Report 95–104 (1995).
[3] R.J. Finch and R.C. Ewing, J. Nucl. Mater. 190 (1992) 133.
[4] E.C. Pearcy, J.D. Prikryl, W.M. Murphy and B.W. Leslie, Appl. Geochem. 9 (1994) 713.
[5] D.J. Wronkiewicz, J.K Bates, T.J Gerding, E. Veleckis and B.S. Tani, J. Nucl. Mater. 190 (1992) 107.
[6] B. Grambow, A. Loida, P. Dressler, H. Geckeis, J. Gago, I. Casas, J. de Pablo, J. Giménez and M.E. Torrero, Forschungszentrum Karlsruhe, Technik und Umwelt, Wissenschaftliche Berichte, FZKA 5702.
[7] P.A. Finn, J.C. Hoh, S.F. Wolf, S.A. Slater and J.K. Bates, Radiochim. Acta 74 (1996) 65.
[8] Ch. Cachoir, M.J. Guittet, J.-P. Gallien and P. Trocellier, Radiochim. Acta 74 (1996) 59.
[9] R.S. Forsyth and L.O. Werme, J. Nucl. Mater. 190 (1992) 3.
[10] R. Wang and Y.B. Katayama, Nucl. Chem. Waste Manage. 3 (1982) 83.
[11] D.E. Hobart, in: Proc. of the Robert A. Welch Foundation, Conf. on Chemical Research XXXIV, Fifty Years with Transuranium Elements, Houston, TX (1990).
[12] V.M. Oversby, in: Materials Sciences and Technology A Comprehensive Treatment, eds. R.W. Chan, P. Haasen and E.J. Kramer (VCH, Germany, 1994).
[13] P.C. Burns, M.L. Miller and R.C. Ewing, Can. Mineral. 34 (1996) 845.
[14] H.T. Evans Jr., Science 141 (1963) 154.
[15] P.C. Burns, R.C. Ewing and F.C. Hawthorne, in preparation.
[16] I.D. Brown, in: Structure and Bonding in Crystals II, eds. M. O'Keeffe and A. Navrotsky (Academic Press, New York, 1981).
[17] M.L. Miller, R.J. Finch, P.C. Burns and R.C. Ewing, J. Mater. Res. 11 (1996) 3048.
[18] J.H. Burns, in: The Chemistry of the Actinide Elements Vol. 2, eds. J.J. Katz, G.T. Seaborg and L.R. Morss, 2nd Ed. (Chapman and Hall, New York, 1986).
[19] M.S. Grigor'ev, I.A. Charushnikova, A.M. Fedoseev, N.A. Budantseva, N.A. Baturin and L. Regel, Radiokhimiya 33 (4) (1991) 19.
[20] N.E. Brese and M. O'Keeffe, Acta Crystallogr. B47 (1991) 192.
[21] R.D. Shannon, Acta Crystallogr. A32 (1976) 751.
[22] P.C. Burns, M.L. Miller, R.C. Ewing, R.J. Finch and F.C. Hawthorne, J. Nucl. Mater., submitted.
[23] B.O. Loopstra, Acta Crystallogr. B26 (1970) 656.
[24] M.K. Pagoaga, D.E. Appleman and J.M. Stewart, Am. Mineral. 72 (1987) 1230.
[25] P.G. Dickens and A.V. Powell, J. Solid State Chem. 92 (1991) 169.
[26] B.O. Loopstra, J. Acta Crystallogr. 17 (1964) 651.
[27] M.M. Granger and J. Protas, Bull. Soc Fr. Mineral. Cristallogr. 88 (1965) 211.
[28] R.J. Finch, M.A. Cooper, F.C. Hawthorne and R.C. Ewing, Can. Mineral. 34 (1996) 1071.
[29] P. Piret, Bull. Mineral. 108 (1985) 659.
[30] F. Demartin, C.M. Gramaccioli and T. Pilati, Acta Crystallogr. C48 (1992) 1.
[31] D. Ginderow, Acta Crystallogr. C44 (1988) 421.
[32] F.V. Stohl and D.K. Smith, Am. Mineral. 66 (1981) 610.
[33] R.R. Ryan and A. Rosenzweig, Cryst. Struct. Commun. 6 (1977) 611.
[34] W.D. Birch, W.G. Mumme and E.R. Segnit, Aust. Mineral. 3 (1988) 125.
[35] G.G. Christoph, A.C. Larson, P.G. Eller, I.D. Purson, J.D. Zahrt, R.A. Penneman and G.H. Rinehart, Acta Crystallogr. B44 (1988) 575.
[36] C. Keller, Kernforschungszentrum Karlsruhe Ber. 225 (1964) 229.
[37] M.S. Grigor'ev, A.I. Yanovskii, A.M. Fedoseev, N.A. Budantseva, Yu T. Struchkov and N.N. Krot, Radiokhimiya 33 (2) (1991) 17.
[38] M.S. Grigor'ev, I.A. Charushnikova, N.N. Krot, A.I. Yanovskii and Yu T. Struchkov, Zh. Neorg. Khim. 39 (1994) 179.
[39] S.V. Tomilin, Y.F. Volkov, R.F. Melkaya, V.I. Spiryakov and I.I. Kapshukov, Radiokhimiya 28 (1986) 695.
[40] A.A. Lychev, L.G. Mashirov, Y.I. Smolin and Y.F. Shepelev, Radiokhimiya 30 (1988) 412.
[41] N.W. Alcock, D.J. Flanders and D. Brown, J. Chem. Soc. Dalton Trans. 1986 (1986) 1403.
[42] N.W. Alcock and M.M. Roberts, Acta Crystallogr. 38 (1982) 1805.
[43] F.H. Ellinger and W.H. Zachariasen, J. Phys. Chem. 58 (1954) 405.
[44] C. Keller, Nukleonik 4 (1962) 271.
[45] M. Taylor and R.C. Ewing, Acta Crystallogr. B34 (1978) 1074.
[46] M. Quarton and A. Kahn, Acta Crystallogr. B35 (1979) 2529.
[47] T.L. Cremers, P.G. Eller, and R.A. Penneman, Acta Crystallogr. C39 (1983) 1165.
[48] M. Huyghe, M.R. Lee, M. Quarton and F. Robert, Acta Crystallogr. C47 (1991) 244.
[49] P. Kroeschell and R. Hoppe, Z. Anorg. Allg. Chem. 509 (1984) 127.
[50] G. Braver and H. Gradinger, Z. Anorg. Allg. Chem. 276 (1954) 209.
[51] A. Tabuteau, A. Cousson and M. Pages, Acta Crystallogr. 35 (1979) 2000.
[52] W.H. Zachariasen, Acta Crystallogr. 2 (1949) 388.
[53] N.C. Jayadevan, K.D. Singh-Mudher and D.M. Chackraburtty, Z. Kristallogr. 161 (1982) 7.
[54] B. McCart, G.H. Lander and A.T. Aldred, J. Chem. Phys. 74 (1981) 5263.
[55] A. Tabuteau and M. Pages, J. Solid State Chem. 26 (1978) 153.
[56] J.H. Burns and R.D. Baybarz, Inorg. Chem. 11 (1972) 2233.
[57] D.H. Templeton and C.H. Dauben, J. Am. Chem. Soc. 75 (1953) 4560.